communications chemistry

Article

https://doi.org/10.1038/s42004-024-01281-5

Absence of a link between stabilized charge-separated state and structural changes proposed from crystal structures of a photosynthetic reaction center

Check for updates

Tomoyasu Noji[1,2], Keisuke Saito[1,2] & Hiroshi Ishikita[1,2]

Structural differences between illuminated and unilluminated crystal structures led to the proposal that the charge-separated state was stabilized by structural changes in its membrane extrinsic protein subunit H in a bacterial photosynthetic reaction center [Katona, G. et al. *Nat. Struct. Mol. Biol*. 2005, 12, 630–631]. Here, we explored the proposal by titrating all titratable sites and calculating the redox potential (E_m) values in these crystal structures. Contrary to the expected charge-separated states, E_m for quinone, $E_m(Q_A/Q_A^{\bullet-})$, is even lower in the proposed charge-separated structure than in the ground-state structure. The subunit-H residues, which were proposed to exhibit electron-density changes in the two crystal structures, contribute to an $E_m(Q_A/Q_A^{\bullet-})$ difference of only <0.5 mV. Furthermore, the protonation states of the titratable residues in the entire reaction center are practically identical in the two structures. These findings indicate that the proposed structural differences are irrelevant to explaining the significant prolongation of the charge-separated-state lifetime.

Photosynthetic reaction centers from purple bacteria (PbRC) share structural similarities with photosystem II (PSII), both classified as type II reaction centers, characterized by their redox-active cofactors in the electron transfer branches[1]. In PbRC, light-induced charge separation initiates electron transfer via accessory bacteriochlorophyll (B_L) to bacteriopheophytin (H_L) in the L branch, while the resulting cationic state is delocalized over the bacteriochlorophyll pair (P_LP_M). Bacteriochlorophyll (B_M) and bacteriopheophytin (H_M) in the M branch do not participate in electron transfer. In PSII, these cofactors are conserved as accessory chlorophyll (Chl_{D1}) and pheophytin ($Pheo_{D1}$) in the active D1 branch and Chl_{D2} and $Pheo_{D2}$ in the inactive D2 branch[2]. Electron transfer further proceeds via the primary quinone (Q_A) to the secondary quinone (Q_B). At an equidistant position from Q_A to Q_B lies the non-heme Fe complex, with four histidine and one carboxylic ligands (HCO_3^- in PSII and Glu-M234 in PbRC)[3]. Following the second electron transfer, doubly protonated Q_BH_2 forms and exits the reaction center towards the quinone pool. Subsequently, an unprotonated, oxidized quinone from the quinone pool enters the Q_B binding site, serving as Q_B in the subsequent turnover.

In PSII, the Q_B binding site is also a target for commercial herbicides. Once a herbicide binds to PSII, forward electron transfer from $Q_A^{\bullet-}$, and therefore photosynthesis, is inhibited[4]. Similarly, inhibition of forward electron transfer from $Q_A^{\bullet-}$ also occurs under strong light. This is because the quinone pool is fully reduced and the Q_B binding site is unoccupied[5,6]. If the gap in redox potential (E_m) between Q_A and $Pheo_{D1}$ is small, backward electron transfer from $Q_A^{\bullet-}$ via $Pheo_{D1}$ to cationic chlorophyll occurs, resulting in triplet chlorophyll and generating harmful singlet oxygen species. To prevent this, PSII upshifts $E_m(Q_A/Q_A^{\bullet-})$ (forming the high potential Q_A conformation[7]) and widens the E_m gap between Q_A and $Pheo_{D1}$. This energetic change allows PSII to use a less harmful, low energy route for charge recombination (photoprotection)[4,8]. The mechanism for the $E_m(Q_A/Q_A^{\bullet-})$ upshift likely involves primarily the loss of the bicarbonate ligand from the non-heme Fe complex[9,10] and, secondarily, the resulting rearrangement of polar H groups[11,12]. The photoaccumulation of $Q_A^{\bullet-}$ leads to the release of the bicarbonate ligand[10] via the channel formed by D1-Tyr246, D1-Ile248, and D2-Phe235[12], resulting in a 70 mV increase in $E_m(Q_A/Q_A^{\bullet-})$[9]. Notably, in PbRC, the bicarbonate ligand is replaced with Glu-M234, and the HCO_3^-/CO_2-releasing channel does not exist due to the presence of membrane-extrinsic subunit H. While the loss of the negative charge itself upshifts $E_m(Q_A/Q_A^{\bullet-})$, it also facilitates the formation of a low-barrier H-bond between D2-His214, a ligand of the non-heme Fe complex, and $Q_A^{\bullet-}$[12]. Given that the pK_a values for the H-bond donor and acceptor moieties are nearly equal in low-barrier H-bonds[13,14],

[1]Department of Applied Chemistry, The University of Tokyo, Bunkyo-ku, Tokyo, 1, Japan. [2]Research Center for Advanced Science and Technology, The University of Tokyo, Meguro-ku, Tokyo, Japan. e-mail: hiro@appchem.t.u-tokyo.ac.jp

the proton of D2-His214 significantly migrates toward $Q_A^{\bullet-}$, effectively stabilizing it[12].

A similar phenomenon involving $Q_A^{\bullet-}$ stabilization is observed in PbRC. Specifically, in Q_B-depleted PbRC, $Q_A^{\bullet-}$ exhibited a lifetime of 100 ms under normal light conditions, which significantly prolonged to 250 s under bright light exposure[15,16]. The rate of charge recombination is sensitive to the energy difference between the charge-separated $[P_LP_M]^{\bullet+}Q_A^{\bullet-}$ and ground $[P_LP_M]^0Q_A^0$ states[16]. It has been suggested that $E_m(Q_A/Q_A^{\bullet-})$ plays a crucial role in determining the charge recombination pathway in PbRC[17–20]. To elucidate the molecular mechanism behind the significantly prolonged lifetime for 250 s of photoaccumulated $Q_A^{\bullet-}$, Katona et al. analyzed the protein crystal structures obtained during continuous bright light illumination at 100 K for 5 minutes[21]. Katona et al. presumed that the illuminated crystal structure reported at a 2.5 Å resolution corresponded to the charge-separated structure (PDB code 2BNS) and the unilluminated structure reported at a 2.7 Å resolution corresponded to the ground-state structure (PDB code 2BNP). Based on their observations of these crystal structures, they highlighted structural changes in a region associated with subunit H, including His-L211, Arg-M13, Arg-M29, His-H68, Arg-H70, Arg-H89, His-H126 and His-H128, and Arg-H189[21] (Fig. 1). They also emphasized that the subdomain from Pro-H121 to Thr-H226, containing 12 positively charged and 12 negatively charged residues, generates a "net electrostatic force" due to interaction with $Q_A^{\bullet-}$ in the charge-separated structure[21]. Furthermore, they proposed that His-H126 and His-H128, known as the Cd^{2+} binding site of the proton-transfer inhibited PbRC[22], could facilitate divalent cation binding upon the formation of long-lived $Q_A^{\bullet-}$, thereby increasing the activation barrier for the charge recombination due to the electrostatic interaction between the divalent cation and $Q_A^{\bullet-}$ over a distance of 25 Å[21].

The proposed mechanism is intriguing and worthy of investigation. However, it differs significantly from the mechanism in PSII, in which $Q_A^{\bullet-}$ stabilization is achieved by the rather local protein environment adjacent to Q_A[9,12]. In addition, as they acknowledged, full conformational change was not expected at low temperature (100 K) during for data collection, and only ~30% of the protein was estimated to be in the charge-separated $Q_A^{\bullet-}$ state[21]. Furthermore, it remains unclear whether their "reproducibly observed" structural changes (via electron density changes) can be appropriately represented in the reported atomic coordinates obtained at resolutions of 2.5 to 2.7 Å.

Here, we investigated the energetics of the redox-active cofactors in the proposed charge-separated and ground-state structures by solving the linear Poisson-Boltzmann equation and considering the protonation states of all titratable sites in the entire protein. Of particular interest are the E_m values derived from the original atomic coordinates of these crystal structures. Given that E_m values are predominantly influenced by protein electrostatics, which are directly reflected in the original atomic coordinates of crystal structures as demonstrated previously (e.g.[23–25]), determining the E_m values of the redox-active cofactors in each structure serves as a crucial initial step in assessing the functional relevance of the proposed charge-separated and ground-state structures to their respective electron-transfer states.

Results and Discussion

Overview of E_m profiles

In both the proposed charge-separated and ground-state structures, the E_m values for B_L and H_L are higher than those for B_M and H_M, respectively, indicative of electron transfer along the L-branch (Fig. 2). These E_m profiles resemble that obtained using a higher resolution structure (2.0 Å; PDB code 3I4D[26])[27]. The relatively small difference between $E_m(B_L)$ and $E_m(B_M)$ (~30 mV), in contrast to the reported difference (~170 mV[27]) for the higher resolution structure, is due to the absence of a carotenoid molecule, spheroidene, near B_M in these crystal structures. The presence of spheroidene increases hydrophobicity near B_M and destabilizes $B_M^{\bullet-}$, decreasing $E_m(B_M)$[27].

The calculated $E_m(Q_A/Q_A^{\bullet-})$ values for the proposed charge-separated and ground-state structures are −146 mV and −133 mV, respectively (Fig. 2), comparable to experimentally measured values of −180 mV for PbRC from *Rhodobacter sphaeroides*[28]. However, no significant differences in the E_m values are observed between the charge-separated and ground-state structures. Notably, $E_m(Q_A/Q_A^{\bullet-})$ in the charge-separated structure, presumed to possess $Q_A^{\bullet-}$, is even slightly lower (13 mV) than in the ground-state structure (Fig. 2). Consequently, $Q_A^{\bullet-}$ is unexpectedly less stable in the charge-separated structure than in the ground-state structure, in contradiction to their originally assumed states. Based on the E_m difference, the structural difference between the charge-separated and ground-state structures falls short of explaining the significant prolongation of the charge-separated-state lifetime from 100 ms to 250 s.

Influences of the proposed key residues on $E_m(Q_A/Q_A^{\bullet-})$

Katona et al. highlighted Arg-M13, Arg-M29, Arg-H70, Arg-H89, and Arg-H189, as contributors to the significant prolongation of the charge-separated-state lifetime from 100 ms to 250 s (Fig. 1). According to their interpretation, these residues exhibited reproducible structural changes in response to bright light[21]. Additionally, they proposed that His-L211 (incorrectly labeled as His-M211 in ref. 21), His-H68, His-H126 and His-H128, were involved in the region electrostatically stabilizing $Q_A^{\bullet-}$[21] (Fig. 1). However, the present analysis indicates that these residues do not practically differentiate $E_m(Q_A/Q_A^{\bullet-})$ between the charge-separated and ground-state structures. Their contributions to the difference in $E_m(Q_A/Q_A^{\bullet-})$ are consistently less than 0.5 mV (Table 1). Moreover, the influences of these residues on $E_m(Q_A/Q_A^{\bullet-})$ are originally minimal, mostly below 5 mV in each structure (Table 1). These results suggest that the residues proposed by Katona et al., including His-L211, Arg-M13, Arg-M29, His-H68, Arg-H70, Arg-H89, His-H126, and His-H128, and Arg-H189, neither distinguish $E_m(Q_A/Q_A^{\bullet-})$ between the two structures nor impact $E_m(Q_A/Q_A^{\bullet-})$ in each structure.

Katona et al. also highlighted the importance of the region from Pro-H121 to Thr-H226 in subunit H, emphasizing that it generates a "net electrostatic force" due to interaction with $Q_A^{\bullet-}$[21]. However, this region, comprising 106 residues, contributes to decreases in $E_m(Q_A/Q_A^{\bullet-})$ of 30 mV for the proposed charge-separated structure and 25 mV for the ground-state structure, resulting in only a 5 mV difference (Table S1). Based on these results, their proposed "charge-separated" structure (PDB code 2BNS) is unlikely to specifically represent the charge-separated state.

Residues that increase $E_m(Q_A/Q_A^{\bullet-})$ in the proposed charge-separated structure with respect to the ground-state structure

Although the proposed charge-separated structure is unlikely to represent the relevant charge-separated state, below we identify residues that stabilize $Q_A^{\bullet-}$ in the proposed charge-separated structure for further clarification of the proposal in ref. 21. Instead of the residues highlighted by Katona et al., the present study identifies Thr-M261 as the primary contributor to $Q_A^{\bullet-}$ stabilization in their proposed charge-separated structure, causing a modest increase in $E_m(Q_A/Q_A^{\bullet-})$ by 11 mV compared to the ground-state structure (Table 2, Fig. 3a). The difference in the $Q_A^{\bullet-}$ stabilization arises from the orientation of its backbone carbonyl group, with the carbonyl O atom being closer to Q_A in the ground-state structure (3.9 Å) than the proposed charge-separated structure (4.1 Å)[21], causing a minor destabilization of $Q_A^{\bullet-}$ in the ground-state structure.

Glu-L212, a residue exhibiting proton uptake (0.3 to 0.8 H^+) upon $Q_B^{\bullet-}$ formation during the electron transfer from Q_A to Q_B[29–33], is more protonated in the proposed charge-separated structure (0.2 H^+) than in the ground-state structure (0.1 H^+). This increased protonation contributes to an 6 mV increase in $E_m(Q_A/Q_A^{\bullet-})$ in the proposed charge-separated structure compared to the ground-state structure (Table 2). Glu-H173, a residue that substitutes a proton-uptake role of Glu-L212 in Glu-L212 mutant PbRCs[34–36], contributes to a 3 mV increase $E_m(Q_A/Q_A^{\bullet-})$ in the proposed charge-separated structure due to the difference in its protonation state (0.1 H^+ in the proposed charge-separated structure and 0 H^+ in the ground-state structure).

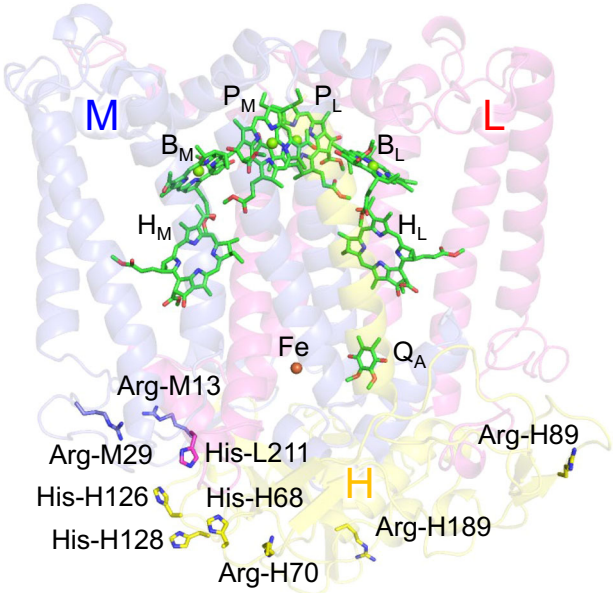

Fig. 1 | Residues proposed to be involved in structural changes in response to bright light in ref. 21.

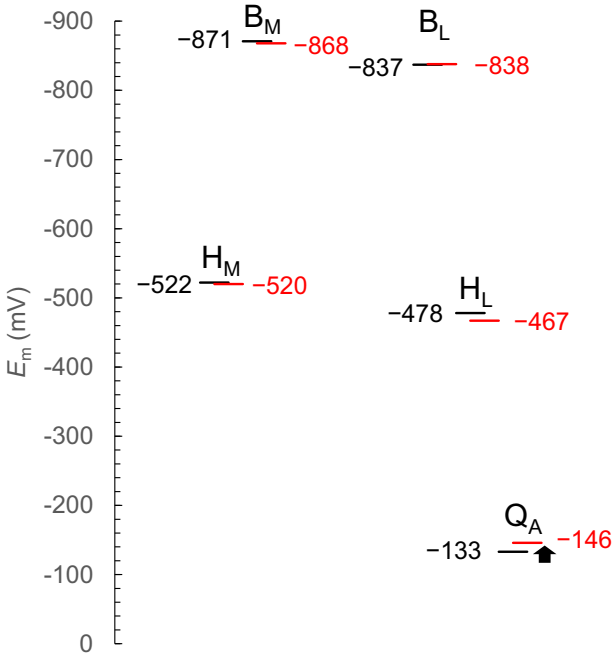

Fig. 2 | E_m profiles for the proposed charge-separated and ground-state structures (i.e., protein crystallography Q_A^0 conformation). Numerical values indicate E_m for each structure (mV). Red bars and numerical values represent E_m for the proposed charge-separated structure, while black bars and numerical values represent E_m for the ground-state structure. The black arrow indicates the observed shift in $E_m(Q_A/Q_A^{\bullet-})$ upon the formation of the proposed charge-separated state.

However, the accumulated influence of these residues on $E_m(Q_A/Q_A^{\bullet-})$ is relatively small, paradoxically resulting in the low $E_m(Q_A/Q_A^{\bullet-})$ value in the proposed charge-separated structure compared to the ground-state structure (Fig. 2).

Notably, none of the residues proposed by Katona et al. (Arg-M13, Arg-M29, His-H68, Arg-H70, Arg-H89, His-H126 and His-H128, and Arg-H189[21]) significantly contribute to $E_m(Q_A/Q_A^{\bullet-})$ differences (Table 2). To explain the prolongation of the charge-separated-state lifetime, Katona et al.

Table 1 | Contribution of residues proposed for $Q_A^{\bullet-}$ stabilization in ref. 21 to $E_m(Q_A/Q_A^{\bullet-})$ in the proposed charge separated and ground-state structures (mV)

	Charge separated	Ground state	Difference
His-L211[a]	1.2	1.2	0.0
Arg-M13	2.5	2.0	0.5
Arg-M29	4.4	4.6	−0.2
His-H68	2.6	2.4	0.2
Arg-H70	10.4	10.8	0.4
Arg-H89	2.6	2.4	0.2
His-H126	1.7	1.9	0.2
His-H128	−0.2	−0.3	0.1
Arg-H189	2.7	2.9	−0.2

For clarity, the first decimal places are shown only in this table.
[a]Labeled as His-M211 in ref. 21, but the corresponding residue does not exist in subunit M. It seems most likely that it corresponds to His-L211.

Table 2 | Residues contributing to $E_m(Q_A/Q_A^{\bullet-})$ increase (more than 4 mV) in the proposed charge-separated structure compared to the ground-state structure (mV)

	Charge separated	Ground state	Difference
Thr-M261	−49	−60	11
Glu-L212	−41	−47	6
Glu-M234	−133	−139	6
Glu-H173	−32	−36	4

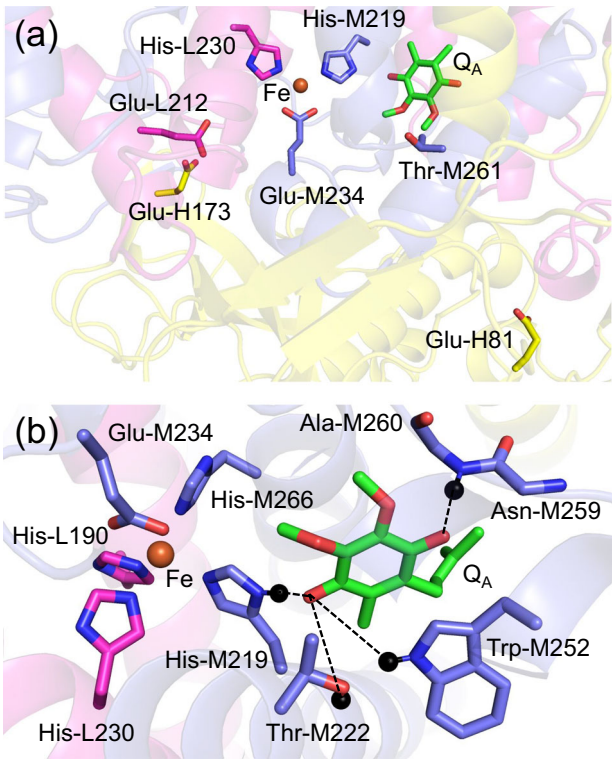

Fig. 3 | Residues near the Q_A binding site. a Residues that increase $E_m(Q_A/Q_A^{\bullet-})$ in the proposed charge-separated structure with respect to the ground-state structure. **b** H-bond network of Q_A. Black balls represent H atoms in the QM/MM-optimized $Q_A^{\bullet-}$ conformation. The dotted lines indicate interactions with the carbonyl O sites of Q_A.

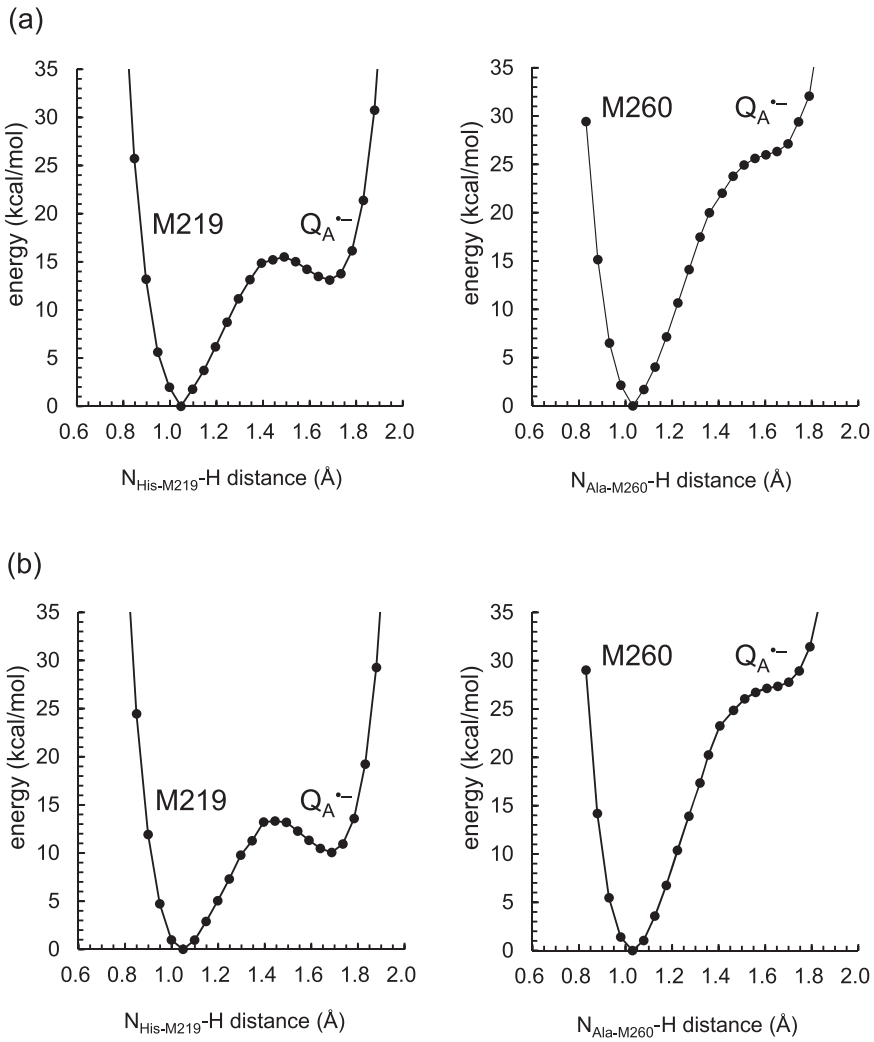

Fig. 4 | Potential energy profiles along H-bonds with $Q_A^{\bullet-}$. a Proposed charge-separated structure. **b** Ground-state structure. Left panels show the profile for the H-bond between $Q_A^{\bullet-}$ and His-M219. The right panels show the profile for the H-bond between $Q_A^{\bullet-}$ and Ala-M260 (backbone amide).

specifically proposed that His-H126 and His-H128, a binding site of Cd^{2+} on the protein bulk surface[22], contributed to $Q_A^{\bullet-}$ stabilization by 14 kJ mol $^{-1}$, despite the considerable distance of ~25 Å. This assumption was based on the presence of a divalent +2 charge on the His-H126/His-H128 site and a medium with a dielectric constant of 4 for the PbRC protein[21]. It has been reported that Cd^{2+} binding at His-H126 and His-H128 leads to reorientations of charged and polar side chains along proton transfer pathways toward Q_B[22,37], an event known as the "electrostatic domino[38]" effect. However, most of the residues involved in this event do not exhibit the structural changes proposed by Katona et al.

It is also crucial to note that proteins, including PbRC, cannot be appropriately considered as a homogeneous medium with a dielectric constant of 4, even if approximated, in contrast to their assumption in ref. 21. Although a dielectric constant of 4 is often applied to the protein interior (i.e., the region originating approximately from van der Waals spheres of protein atoms) in theoretical studies, this procedure does not result in a uniform medium with a dielectric constant of 4 due to the presence of the bulk or cavity water regions with a dielectric constant of 80 (e.g. ref. 39). In particular, His-H126 and His-H128 are exposed to the protein bulk surface, and the electrostatic influence of the divalent ion at His-H126/His-H128 on $Q_A^{\bullet-}$ is significantly screened (Table 1). Therefore, their assumption of a 14 kJ mol^{-1} electrostatic interaction between the divalent ion and $Q_A^{\bullet-}$ is overestimated and unlikely to explain the notable prolongation of the charge-separated-state lifetime from 100 ms to 250 s.

Exploring an alternative mechanism for $Q_A^{\bullet-}$ stabilization (1): Energetics of $Q_A^{\bullet-}$ protonation in the proposed charge-separated structure

If $Q_A^{\bullet-}$ were overstabilized, potential $Q_A^{\bullet-}$ protonation might contribute to the absence of structural features representing the charge-separated state in the proposed charge-separated structure. Indeed, the formation of protonated Q_A due to excessive electron transfer in the absence of Q_B under high light has been suggested for photosystem II (PSII)[5,6], although, to the best of our knowledge, it has not been specifically reported for PbRC. In PbRC, the Q_A carbonyl O site proximal to the non-heme Fe complex (proximal O site) forms an H-bond with His-M219, the ligand of the non-heme Fe complex, while the Q_A carbonyl O site distal to the non-heme Fe complex (distal O site) forms an H-bond with the backbone amide group of Ala-M260.

To explore the possibility of $Q_A^{\bullet-}$ protonation in the proposed charge-separated structure, the potential-energy profile for the H-bonds between $Q_A^{\bullet-}$ and its H-bond partners are analyzed, as protonation of quinone requires the release of protons from H-bond partners (e.g., Q_B in PbRC[40] and PSII[41]). The potential-energy profile indicates that the release of the proton from His-M219 to the proximal O site of $Q_A^{\bullet-}$ is significantly uphill in the proposed charge-separated structure, i.e., pK_a(His-M219) >> pK_a($Q_A^{\bullet-}$/ $Q_AH^{\bullet}$). Furthermore, the release of a proton from Ala-M260 to the distal O site of $Q_A^{\bullet-}$ is more significantly uphill in the proposed charge-separated structure (Fig. 4a). No substantial difference in the potential-energy profile is observed in the ground-state structure (Fig. 4b), which suggests that the proposed charge-separated structure is not substantially

Table 3 | pK_a values for titratable residues near quinones in the proposed charge-separated and ground-state structures

	Charge separated		Ground state	
	Q_A^0	$Q_A^{\bullet-}$	Q_A^0	$Q_A^{\bullet-}$
Asp-L210	4.9	5.0	5.8	6.0
Glu-L212	6.3	6.8	6.1	6.5
Asp-L213	7.4	7.2	7.7	7.5
Asp-M17	5.9	6.1	5.8	6.1
Asp-M240	6.1	6.1	6.1	6.0
His-H68	6.4	6.3	6.2	6.2
Asp-H124	4.8	4.8	4.6	4.5
His-H126	7.1	7.1	7.1	7.1
His-H128	7.7	7.7	7.7	7.7
Asp-H170	−4.2	−4.1	−2.5	−2.3
Glu-H173	6.2	6.3	5.6	5.8
Glu-H224	4.3	4.3	4.4	4.4

The locations of these residues are summarized in ref. 43.

Table 4 | Protonation states of residues that exhibit significant changes in the protonation state for the $Q_A^{\bullet-}$ state of the proposed charge-separated structure with respect to the Q_A^0 state of the ground-state structure ([H^+])

	Charge separated $Q_A^{\bullet-}$	Ground state Q_A^0	Difference
Glu-H79	0.59	0.39	0.20
Glu-L212	0.25	0.10	0.15
Glu-M236	0.72	0.66	0.06
Asp-M17	0.10	0.06	0.04
Asp-L213	0.75	0.84	−0.09

distinct from the ground-state structure even in this context. The significant uphill proton transfer observed for $Q_A^{\bullet-}$ contrasts sharply with the downhill (distal O site) or isoenergetic (proximal O site) proton transfer toward $Q_B^{\bullet-}$ or Q_BH^- in PbRC[40] and PSII[41]. Therefore, unless unusual structural changes such as protein denaturation occur, it seems unlikely that protonation of $Q_A^{\bullet-}$ occurs in PbRC.

In PSII, when exposed to high light, $Q_A^{\bullet-}$ protonation occurs by the release of the proton from D2-His214 (equivalent to His-M219 in PbRC), concomitant with the loss of the bicarbonate ligand from the non-heme Fe complex. The loss of the negatively charged bicarbonate ligand decreases pK_a(D2-His214), resulting in pK_a(D2-His214) ≈ pK_a($Q_A^{\bullet-}$/ $Q_AH^\bullet$) and the formation of a low-barrier H-bond between D2-His214 and $Q_A^{\bullet-}$, facilitating proton transfer[12]. The increase in E_m($Q_A/Q_A^{\bullet-}$) upon the loss of the bicarbonate ligand[9] is attributed not only to the elimination of the direct electrostatic interaction between the anionic bicarbonate ligand and $Q_A^{\bullet-}$ but also to the low-barrier H-bond, which promotes the migration of the D2-His214 proton towards the $Q_A^{\bullet-}$ moiety. However, in PbRC, the corresponding acidic ligand is Glu-M234, which remains bound as part of the polypeptide M chain. Thus, the inability to release the bicarbonate ligand from the non-heme Fe complex suggests that $Q_A^{\bullet-}$ protonation is less relevant in PbRC.

Exploring an alternative mechanism for $Q_A^{\bullet-}$ stabilization (2): pK_a for titratable residues near quinones

Protonation states of titratable residues near Q_B, specifically Glu-L212 and Asp-L213, play a crucial role in altering E_m(Q_B)[42], although a corresponding cluster of titratable residues is absent on the Q_A side. Nevertheless, if the protonation states of these residues near Q_B differed between the proposed charge-separated and ground-state structures, substantial differences might lead to variations in E_m(Q_A). However, the calculated pK_a values for the titratable residues near quinones (e.g., summarized in ref. 43) are substantially identical between the two structures (Table 3). Note that the resulting protonation states for Glu-L212 and Asp-L213 are consistent with those reported previously[23,24,42] based on other crystal structures (PDB codes, 1AIG and 1AIJ[44]). In addition, the total charges of all titratable residues in the entire protein structures are: −0.67 for Q_A^0 and −0.34 for $Q_A^{\bullet-}$ in the proposed charge-separated structure, and −0.72 for Q_A^0 and −0.32 for $Q_A^{\bullet-}$ in the ground-state structure. The total charge of the titratable residues slightly decreases in response to $Q_A^{\bullet-}$ formation due to partial proton uptake (e.g., by Glu-L212, Table 3). However, no significant difference in the protonation pattern is observed between the two structures. These results suggest that the proposed charge-separated structure does not rationalize the stabilization of $Q_A^{\bullet-}$ compared to the ground-state structure.

Alternatively, it is also meaningful to identify the titratable residues undergoing notable changes in protonation state between the $Q_A^{\bullet-}$ state of the proposed charge-separated structure and the Q_A^0 state of the ground-state structure (Table 4). The present analysis reveals such residues to include Glu-H79 (uptake of 0.2 H^+ upon $Q_A^{\bullet-}$ formation, 15 Å from Q_A), Glu-L212 (0.2 H^+, 14 Å from Q_A), and Asp-L213 (−0.1 H^+, 19 Å from Q_A), albeit with minor alterations in protonation state. Many of these residues, such as Glu-L212, Asp-L213, and Asp-M17) are involved in protonation events for Q_B (e.g.[40,43],). However, none of these residues, including Glu-H79, are among those proposed by Katona et al. as stabilizing $Q_A^{\bullet-}$ (His-L211, Arg-M13, Arg-M29, His-H68, Arg-H70, Arg-H89, His-H126 and His-H128, and Arg-H189[21]) or generating a "net electrostatic force" interacting with $Q_A^{\bullet-}$ (from Pro-H121 to Thr-H226[21]). Therefore, their proposal lacks support from the electrostatics originating from their own reported structures.

Katona et al. also proposed a mechanism for $Q_A^{\bullet-}$ stabilization, facilitated by "several ordered water molecules" located between Q_A-binding pocket and the C-terminal region of subunit H[21]. According to their proposal, light-induced conformational changes in subunit H increase the cavity size for these water molecules, causing them to become disordered and increasing the dielectric constant of the water cavity. They proposed that "a transition from ordered to disordered water would allow water molecules to orient their dipole moments" to stabilize $Q_A^{\bullet-}$[21]. However, this contradicts the general understanding that increasing the disorder of water molecules around a charged group results in their random orientations, which effectively screen electrostatic interactions with the charged group but simultaneously decrease the magnitude of their total dipole moment. Specifically, their statement "a transition from ordered to disordered water would allow water molecules to orient their dipole moments" is logically inconsistent. Instead, it would cause the water molecules to fluctuate, diminishing their total dipole moment. Consequently, the proposal appears to need reconsideration.

Exploring an alternative mechanism for $Q_A^{\bullet-}$ stabilization (3): side-chain reorientation near Q_A

Remarkably, when the PbRC structure is equilibrated with the $Q_A^{\bullet-}$ state (protein crystallography $Q_A^{\bullet-}$ conformation) in the present calculation, E_m($Q_A/Q_A^{\bullet-}$) exhibits an increase of 39 mV with respect to the protein crystal structure of the proposed charge-separated structure (protein crystallography Q_A^0 conformation) (Fig. 5). To unravel the molecular origin of the $Q_A^{\bullet-}$ stabilization in the protein crystallography $Q_A^{\bullet-}$ conformation, the electrostatic contributions of the residues to E_m($Q_A/Q_A^{\bullet-}$) are analyzed. In the protein crystallography $Q_A^{\bullet-}$ conformation, residues that have been reported to be involved in the H-bond network of Q_A, namely Thr-M222, Trp-M252, Ala-M260, and His-M219[45,46], contribute to the $Q_A^{\bullet-}$ stabilization (Tables 5 and 6). Specifically, Thr-M222 and Trp-M252 stabilize $Q_A^{\bullet-}$ more significantly in the $Q_A^{\bullet-}$ conformation than in the protein

crystallography Q_A^0 conformation, as suggested previously for the stabilization of photoaccumulated $Q_A^{\bullet-}$[11]. In the proposed charge-separated structure, Trp-M252 donates an H-bond to Thr-M222. Although the O…O distance between Thr-M222 and Q_A (3.8 Å[21]) is longer than that for a standard H-bond, its hydroxyl H atom migrates toward the proximal carbonyl O atom of Q_A. In the equilibrium with $Q_A^{\bullet-}$, the proton of Thr-M222 more significantly migrates toward the carbonyl O atom of Q_A, providing additional electrostatic stabilization (Tables 5 and 6). Similarly, other residues in the H-bond network of Q_A contribute weak stabilizations to $Q_A^{\bullet-}$ in the protein crystallography $Q_A^{\bullet-}$ conformation compared to the protein crystallography Q_A^0 conformation, collectively resulting in a 39 mV upshift in $E_m(Q_A/Q_A^{\bullet-})$ (Table 5, Fig. 5).

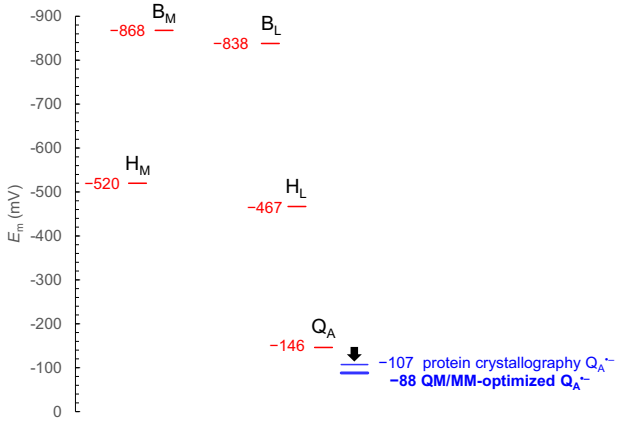

Fig. 5 | Comparison of E_m between the Q_A^0 and $Q_A^{\bullet-}$ conformations. Numerical values indicate E_m for each structure (mV). Red bars and numerical values represent E_m for the proposed charge-separated structure (i.e., protein crystallography Q_A^0 conformation). The blue bar and numerical value represent E_m for the protein crystallography $Q_A^{\bullet-}$ conformation, while the blue thick bar and bold numerical value represent E_m for the QM/MM-optimized $Q_A^{\bullet-}$ conformation. The black arrow indicates the observed shift in $E_m(Q_A/Q_A^{\bullet-})$ upon the formation of the $Q_A^{\bullet-}$ conformation.

Table 5 | Residues contributing to $E_m(Q_A/Q_A^{\bullet-})$ increase (more than 3 mV) in the protein crystallography Q_A^0 conformation compared to the protein crystallography $Q_A^{\bullet-}$ conformation of the proposed charge-separated structure (mV)

	Protein crystallography		QM/MM-optimized
	Q_A^0	$Q_A^{\bullet-}$	$Q_A^{\bullet-}$
Thr-M222	26	35 (9)	34 (8)
Trp-M252	25	34 (9)	32 (7)
Ala-M260	45	48 (4)	53 (8)
His-M219	171	174 (3)	178 (7)

Values in the QM/MM-optimized $Q_A^{\bullet-}$ conformation are shown for comparison. Values in brackets indicate differences from the protein crystallography Q_A^0 conformation.

To explore the possible existence of a conformation that further stabilizes $Q_A^{\bullet-}$, QM/MM calculations are performed, allowing relaxation of atomic coordinates in the entire H-bond network of Q_A (i.e., His-M219, Thr-M222, Trp-M252, and Ala-M260), including the heavy atom positions (Fig. 3b). The QM/MM-optimized $Q_A^{\bullet-}$ conformation (SI coordinate) does not significantly differ from the protein crystallography $Q_A^{\bullet-}$ conformation. The calculated $E_m(Q_A/Q_A^{\bullet-})$ for the QM/MM-optimized $Q_A^{\bullet-}$ conformation exhibits a 58 mV upshift from the protein crystallography Q_A^0 conformation, comparable to the 39 mV upshift observed for the formation of the protein crystallography $Q_A^{\bullet-}$ conformation (Fig. 5). These results suggest that the heavy atom positions of an actual $Q_A^{\bullet-}$ conformation closely resemble those in the protein crystal structure, highlighting that the rearrangement of polar H atom positions, especially at the Q_A binding moiety, likely plays a crucial role in $Q_A^{\bullet-}$ stabilization, as suggested in theoretical studies[11] and electron-nuclear double resonance (ENDOR) spectroscopies[47].

The role of Thr-M222 in providing additional electrostatic stabilization to $Q_A^{\bullet-}$ has long been discussed. In 1994, based on the observations from PbRC crystal structures, Brudler et al. proposed a possible flipping H-bond to Q_A[48], either from His-M219[46] or Thr-M222[45]. In theoretical studies using the light-adapted PbRC structure, a reorientation of the hydroxyl group of Thr-M222 toward $Q_A^{\bullet-}$, along with an increase in $E_m(Q_A/Q_A^{\bullet-})$, was observed in the equilibrium with $Q_A^{\bullet-}$ and put forwarded as the mechanism stabilizing photoaccumulated, long-lived $Q_A^{\bullet-}$[11]. Later, using ENDOR spectroscopies, Flores et al. interpreted that ^{2}H ENDOR lines observed in the region between 7.8 and 8.5 MHz arise from residues adjacent to $Q_A^{\bullet-}$, including Thr-M222 and Trp-M252[47].

Working model

Considering these findings, the rearrangement of polar residues (Table 5) appears to be a more relevant mechanism for stabilizing $Q_A^{\bullet-}$ compared to the structural changes in residues proposed by Katona et al. (Fig. 6). Indeed, the 58 mV increase in $E_m(Q_A/Q_A^{\bullet-})$ calculated upon $Q_A^{\bullet-}$ formation (QM/MM-optimized $Q_A^{\bullet-}$ conformation, Fig. 5) is significantly larger than the 13 mV decrease in $E_m(Q_A/Q_A^{\bullet-})$ observed from the ground state to the charge-separated state in the crystal structures reported by Katona et al. (Fig. 2).

Intriguingly, based on the $Q_A^{\bullet-}$ electron paramagnetic resonance (EPR) signal, which arises from the spin-spin interaction between $Q_A^{\bullet-}$ and Fe^{2+}, it has been suggested that in PSII, there are two energetically different forms of $Q_A^{\bullet-}$, likely caused by differences in the strength of H-bond interactions[49]. Since EPR signals are sensitive to the local environment of the spin rather than the distant environment[50], the EPR results in PSII suggest the residues adjacent to Q_A (rather than those in subunit H in PbRC) are involved in $Q_A^{\bullet-}$ stabilization. This finding aligns with the rearrangement of local polar residues stabilizing $Q_A^{\bullet-}$ observed in the present QM/MM calculations.

Furthermore, the 58 mV increase in $E_m(Q_A/Q_A^{\bullet-})$ upon the formation of photoaccumulated $Q_A^{\bullet-}$ in PbRC is comparable to the 70 mV increase in $E_m(Q_A/Q_A^{\bullet-})$ observed upon the formation of photoaccumulated $Q_A^{\bullet-}$ in PSII[9]. In PSII, the $E_m(Q_A/Q_A^{\bullet-})$ upshift is associated with photoprotection,

Table 6 | H-bond distances with carbonyl O sites of Q_A in the proposed charge-separated structure and the QM/MM-optimized $Q_A^{\bullet-}$ conformation (Å)

	Protein crystallography Q_A^0		QM/MM-optimized $Q_A^{\bullet-}$	
	N…O O…O	H…O	N…O O…O	H…O
His-M219-**NH…O** = C-Q_A	2.80	1.79	2.74 (-0.06)	1.70 (-0.09)
Thr-M222-**OH…O** = C-Q_A	3.79	4.00	3.88 (0.09)	4.04 (0.04)
Trp-M252-**NH…O** = C-Q_A	4.38	4.06	4.61 (0.23)	3.97 (-0.09)
Ala-M260-**NH…O** = C-Q_A	2.88	1.95	2.76 (-0.12)	1.75 (-0.20)

H atoms in the protein crystal structure were generated and energetically optimized using CHARMM[54]. Values in brackets indicate differences from the protein crystallography Q_A^0 conformation.

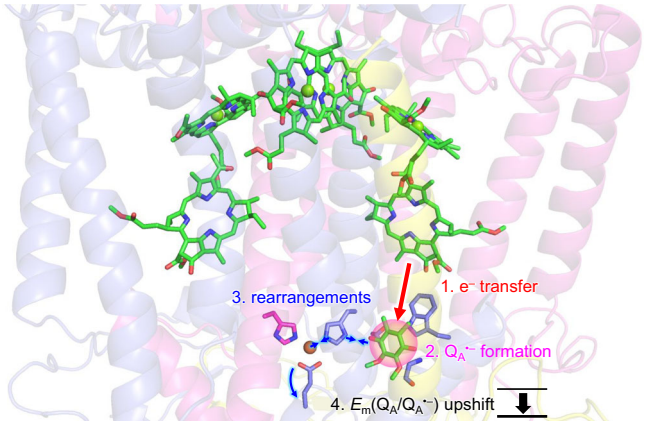

Fig. 6 | Mechanism for the stabilization of $Q_A^{\bullet-}$ through rearrangements of polar groups. The red arrow with the pink circle indicates $Q_A^{\bullet-}$ formation via electron transfer. Blue arrows indicate representative rearrangements of polar groups, with the upshift in $E_m(Q_A/Q_A^{\bullet-})$ caused by these rearrangements indicated by the black arrow.

achieving an increased E_m gap between Q_A and pheophytin. This upshift inhibits backward electron transfer, preventing the formation of harmful triplet chlorophyll species[4,8]. In PSII, the $E_m(Q_A/Q_A^{\bullet-})$ upshift is facilitated by the release of the bicarbonate ligand at the non-heme Fe complex[9,10], leading to the formation of a low-barrier H-bond between Q_A and D2-His214 (corresponding to His-M219 in PbRC) and stabilization of $Q_A^{\bullet-}$[12]. Thus, the upshift in $E_m(Q_A/Q_A^{\bullet-})$ observed in PSII is also substantially due to rearrangement of the polar H group, the proton migrated from D2-His214 along the H-bond stabilizing $Q_A^{\bullet-}$. Considering that PSII achieves the stabilization of photoaccumulated $Q_A^{\bullet-}$ even in the absence of subunit H, it seems plausible that the rearrangement of the polar H group at the Q_A binding site, rather than movements of subunit H, commonly underlies the mechanism in both PSII and PbRC.

In PSII, the formation of $Q_A^{\bullet-}$ facilitates the bidentate-to-monodentate reorientation of the bicarbonate ligand, leading to its release from the non-heme Fe complex[12,51,52]. In the present QM/MM calculation, a similar tendency, namely the bidentate-to-monodentate reorientation of the Glu-M234 ligand and the concomitant shortening of the H-bond between Q_A and His-M219, is also observed upon $Q_A^{\bullet-}$ formation in PbRC (Table S2, Fig. 6). Given that the corresponding ligand, Glu-M234, cannot be released from PbRC, the $E_m(Q_A/Q_A^{\bullet-})$ upshift may be predominantly caused by polar H group rearrangements, which explains the smaller upshift compared to PSII, this somewhat smaller $E_m(Q_A/Q_A^{\bullet-})$ upshift may not be significantly crucial for PbRC, as PbRC does not evolve triplet dioxygen, which forms harmful singlet oxygen species upon charge recombination.

Conclusions

The overall E_m profiles, including $E_m(Q_A/Q_A^{\bullet-})$, for both the proposed charge-separated and ground-state structures (Fig. 2) resemble that reported for the higher resolution structure (PDB code 3I4D[26])[27]. However, $E_m(Q_A/Q_A^{\bullet-})$ in the proposed charge-separated structure (PDB code 2BNS[21]) is lower than in the ground-state structure (PDB code 2BNP[21]), arguing against the 2BNS structure rationalizing the stabilization of $Q_A^{\bullet-}$. The residues proposed by Katona et al. as stabilizing $Q_A^{\bullet-}$ and explaining prolongation of the charge-separated-state lifetime from 100 ms to 250 s (i.e., His-L211, Arg-M13, Arg-M29, His-H68, Arg-H70, Arg-H89, His-H126 and His-H128, and Arg-H189, Fig. 1) do not differentiate $E_m(Q_A/Q_A^{\bullet-})$ between the charge-separated and ground-state structures (Table 1). Katona et al. hypothesized that the region from Pro-H121 to Thr-H226 in subunit H generates a "net electrostatic force" interacting with $Q_A^{\bullet-}$[21]. However, this region contributes to decreases in $E_m(Q_A/Q_A^{\bullet-})$ of 30 mV for the proposed charge-separated structure and 25 mV for the ground-state structure, resulting in a marginal difference of only 5 mV (Table S1). Additionally, despite acknowledging that "the full conformational change was not expected at low temperatures[21]", the direction of the E_m shift caused by this region for the proposed charge-separated structure (5 mV lower than in the ground-state structure, Table S1) contradicts the characteristics expected for the charge-separated state with long-lived $Q_A^{\bullet-}$. This suggests that the small structural displacement observed in the proposed charge-separated structure likely fails to capture the expected characteristics of $Q_A^{\bullet-}$ stabilization, thus falling short of explaining the significant prolongation of the charge-separated-state lifetime from 100 ms to 250 s.

The significant uphill proton transfer observed for $Q_A^{\bullet-}$ in both the proposed charge-separated and ground-state structures suggest that protonation of $Q_A^{\bullet-}$ is unlikely to occur in the PbRC structures (Fig. 4). The calculated pK_a values for the titratable residues near quinones (e.g., summarized in ref. 43) are substantially identical between the two structures (Table 3), which does not result in variations in $E_m(Q_A)$.

Alternatively, rearrangements of polar residues, specifically at the Q_A binding moiety (Fig. 3b), may play a more crucial role in stabilizing photoaccumulated $Q_A^{\bullet-}$, leading to an up to 58 mV increase in $E_m(Q_A/Q_A^{\bullet-})$ (Fig. 5), as implied by theoretical studies[11] and ENDOR spectroscopies[47] (Fig. 6). Such rearrangements of polar H groups cannot be deduced solely from protein crystal structures, especially at low resolutions. This is particularly evident when comparing differences between the two structures reported at resolutions of 2.5 and 2.7 Å as done in ref. 21. A mechanism derived from the energetics of the protein structures obtained at reasonable resolutions and under relevant conditions (e.g., appropriate temperatures in this case), will serve as a basis for understanding the link between light-induced electron transfer and associated protein dynamics.

Methods

Coordinates and atomic partial charges

The atomic coordinates used in the present study were obtained from the protein crystallography of *Rhodobacter sphaeroides* PbRC, specifically the charge-separated structure (PDB code 2BNS) and the ground-state structure (PDB code 2BNP)[21]. Atomic partial charges of amino acids were adopted from the all-atom CHARMM22[53] parameter set. The atomic charges of cofactors, including bacteriochlorophyll *a* (BChl*a*), bacteriopheophytin *a* (BPheo*a*), the non-heme Fe complex, and ubiquinone, were obtained from previous studies on *Rhodobacter sphaeroides* PbRC[27]. The positions of all heavy atoms were fixed, and all titratable groups, such as acidic and basic groups, were ionized during the optimization of the positions of H atoms with CHARMM[54]. According to the protocol[55], the resulting atomic coordinates were then used for subsequent calculations of protonation patterns and redox potentials. All water molecules assigned in the crystal structure were removed for calculations of protonation pattern and redox potential (treated implicitly using a dielectric constant of 80)[55], whereas they were included in QM/MM calculations (treated explicitly).

Protonation pattern

The protonation pattern of the titratable residues and the redox potentials of the redox-active groups were calculated by solving the linear Poisson-Boltzmann equation with the MEAD program[56]. To ensure direct comparisons with previous computational results (e.g. refs. 25,27), identical computational conditions and parameters were used; all computations were performed at 300 K, pH 7.0, and an ionic strength of 100 mM. The dielectric constants of 4 for the protein interior and 80 for water molecules were used. pK_a values of titratable sites in the protein were determined by adding the calculated pK_a difference between the protein site and the reference system to the known reference pK_a value. Experimentally measured pK_a values used as references were 12.0 for Arg, 4.0 for Asp, 9.5 for Cys, 4.4 for Glu, 10.4 for Lys, 9.6 for Tyr[57], and 7.0 and 6.6 for the N_ε and N_δ atoms of His, respectively[58–60]. All other titratable sites were fully equilibrated to the protonation state of the target site during titration. Protonation patterns were sampled using a Monte Carlo method with Karlsberg[61]. The linear Poisson-Boltzmann equation was solved through a three-step grid-focusing

procedure at resolutions of 2.5 Å, 1.0 Å, and 0.3 Å. Monte Carlo sampling provided the probabilities ([protonated] and [deprotonated]) for the two protonation states. The pK_a value was evaluated using the Henderson-Hasselbalch equation.

E_m calculation: solving the linear Poisson-Boltzmann equation

To determine the E_m values in the protein, the electrostatic energy difference between the two redox states in a reference model system was calculated, by solving the linear Poisson-Boltzmann equation with the MEAD program[62]. Experimentally measured E_m values used as references were E_m(BChl*a*/BChl*a*$^{\bullet-}$) = –641 mV, E_m(BPheo*a*/BPheo*a*$^{\bullet-}$) = –384 mV (based on E_m(BChl*a*/BChl*a*$^{\bullet-}$) = –830 mV and E_m(BPheo*a*/BPheo*a*$^{\bullet-}$) = –600 mV for one-electron reduction measured in tetrahydrofuran[63], considering the solvation energy difference). The E_m(Q_A/$Q_A^{\bullet-}$) value was calculated, using the reference E_m value of –163 mV versus NHE for ubiquinone-1 in water[64]. The difference in the E_m value of the protein relative to the reference system was added to the known E_m value, while titrating all titratable residues. Monte Carlo sampling provided probabilities ([A_{ox}] and [A_{red}]) for the two redox states of molecule *A*. E_m was evaluated using the Nernst equation. A bias potential was applied to equalize both redox states ([A_{ox}] = [A_{red}]), yielding the redox midpoint potential as the resulting bias potential.

Quantum mechanical/molecular mechanical (QM/MM) calculations

While the present calculations were aimed to investigate the original atomic coordinates of the proposed charge-separated and ground-state structures and therefore the E_m values were calculated using the original atomic coordinates of these crystal structures, QM/MM calculations were performed to further investigate the PbRC conformation equilibrated with the $Q_A^{\bullet-}$ state (QM/MM-optimized $Q_A^{\bullet-}$ conformation) using the proposed charge-separated structure (SI coordinate). For comparison, the QM/MM-optimized geometry for the PbRC conformation with charge-neutral Q_A^0 (QM/MM-optimized Q_A^0 conformation) was also obtained using the proposed charge-separated structure (SI coordinate). When obtaining QM/MM-optimized geometry, the resulting protonation pattern was implemented explicitly in the titratable residues in the MM region (as the fully protonated or fully deprotonated residues) in the presence of explicit water molecules. The unrestricted density functional theory (DFT) method was employed with the B3LYP functional and LACVP* basis sets using the QSite[65] program. The QM region was defined as Q_A, the non-heme Fe complex (high-spin Fe^{2+}, sidechains of Glu-M234, His-L190, His-L230, His-M219, and His-M266), and the H-bond network (sidechains of His-M219, Thr-M222, and Trp-M252, and backbone groups of Asn-M259 and Ala-M260). All atomic coordinates were fully relaxed in the QM region. In the MM region, the positions of H atoms were optimized using the OPLS2005 force field[66], while the positions of the heavy atoms were fixed. See the Supporting Information for the atomic coordinates of the QM/MM-optimized structures.

Data availability

Electrostatic contributions of residues from Pro-H121 to Thr-H226 to E_m(Q_A/$Q_A^{\bullet-}$) (Table S1), distances between ligand groups and Fe^{2+} in the non-heme Fe complex (Table S2), and changes in distances upon the formation of $Q_A^{\bullet-}$ (Fig. S1) are provided in Supplementary Data 1. Coordinates for QM/MM-optimized structures are provided in Supplementary Data 2 (SI coordinates).

Received: 3 March 2024; Accepted: 22 August 2024;
Published online: 30 August 2024

References

1. Michel, H. & Deisenhofer, J. Relevance of the photosynthetic reaction center from purple bacteria to the structure of photosystem II. *Biochemistry* **27**, 1–7 (1988).
2. Shen, J. R. The structure of photosystem II and the mechanism of water oxidation in photosynthesis. *Annu. Rev. Plant. Biol.* **66**, 23–48 (2015).
3. Muh, F., Glockner, C., Hellmich, J. & Zouni, A. Light-induced quinone reduction in photosystem II. *Biochim. Biophys. Acta* **1817**, 44–65 (2012).
4. Rutherford, A. W. & Faller, P. The heart of photosynthesis in glorious 3D. *Trends Biochem. Sci.* **26**, 341–344 (2001).
5. Vass, I. et al. Reversible and irreversible intermediates during photoinhibition of photosystem II: stable reduced Q_A species promote chlorophyll triplet formation. *Proc. Natl. Acad. Sci. USA* **89**, 1408–1412 (1992).
6. Noguchi, T. Dual role of triplet localization on the accessory chlorophyll in the photosystem II reaction center: photoprotection and photodamage of the D1 protein. *Plant Cell Physiol.* **43**, 1112–1116 (2002).
7. Krieger-Liszkay, A. & Rutherford, A. W. Influence of herbicide binding on the redox potential of the quinone acceptor in photosystem II: relevance to photodamage and phytotoxicity. *Biochemistry* **37**, 17339–17344 (1998).
8. Rutherford, A. W., Osyczka, A. & Rappaport, F. Back-reactions, short-circuits, leaks and other energy wasteful reactions in biological electron transfer: redox tuning to survive life in O_2. *FEBS Lett.* **586**, 603–616 (2012).
9. Brinkert, K., De Causmaecker, S., Krieger-Liszkay, A., Fantuzzi, A. & Rutherford, A. W. Bicarbonate-induced redox tuning in Photosystem II for regulation and protection. *Proc. Natl. Acad. Sci. USA* **113**, 12144–12149 (2016).
10. Shevela, D., Do, H.-N., Fantuzzi, A., Rutherford, A. W. & Messinger, J. Bicarbonate-mediated CO_2 formation on both sides of Photosystem II. *Biochemistry* **59**, 2442–2449 (2020).
11. Ishikita, H. & Knapp, E.-W. Control of quinone redox potentials in photosystem II: electron transfer and photoprotection. *J. Am. Chem. Soc.* **127**, 14714–14720 (2005).
12. Sugo, Y. & Ishikita, H. Proton-mediated photoprotection mechanism in photosystem II, *Front. Plant. Sci*. **13**. (2022).
13. Warshel, A., Papazyan, A. & Kollman, P. A. On low-barrier hydrogen bonds and enzyme catalysis. *Science* **269**, 102–106 (1995).
14. Schutz, C. N. & Warshel, A. The low barrier hydrogen bond (LBHB) proposal revisited: the case of the Asp…His pair in serine proteases. *Proteins* **55**, 711–723 (2004).
15. Andréasson, U. & Andréasson, L.-E. Characterization of a semi-stable, charge-separated state in reaction centers from *Rhodobacter sphaeroides*. *Photosynth. Res.* **75**, 223–233 (2003).
16. Allen, J. P., Chamberlain, K. D. & Williams, J. C. Identification of amino acid residues in a proton release pathway near the bacteriochlorophyll dimer in reaction centers from *Rhodobacter sphaeroides*. *Photosynth. Res.* **155**, 23–34 (2023).
17. Gopher, A. et al. The effect of an applied electric field on the charge recombination kinetics in reaction centers reconstituted in planar lipid bilayers. *Biophys. J.* **48**, 311–320 (1985).
18. Woodbury, N. W., Parson, W. W., Gunner, M. R., Prince, R. C. & Dutton, P. L. Radical-pair energetics and decay mechanisms in reaction centers containing anthraquinones, naphthoquinones or benzoquinones in place of ubiquinone. *Biochim. Biophys. Acta* **851**, 6–22 (1986).
19. Shopes, R. J. & Wraight, C. A. Charge recombination from the $P^+Q_A^-$ state in reaction centers from *Rhodopseudomonas viridis*. *Biochim. Biophys. Acta* **893**, 409–425 (1987).
20. Fufezan, C., Zhang, C., Krieger-Liszkay, A. & Rutherford, A. W. Secondary quinone in photosystem II of *Thermosynechococcus elongatus*: semiquinone-iron EPR signals and temperature dependence of electron transfer. *Biochemistry* **44**, 12780–12789 (2005).

21. Katona, G. et al. Conformational regulation of charge recombination reactions in a photosynthetic bacterial reaction center. *Nat. Struct. Mol. Biol.* **12**, 630–631 (2005).
22. Axelrod, H. L., Abresch, E. C., Paddock, M. L., Okamura, M. Y. & Feher, G. Determination of the binding sites of the proton transfer inhibitors Cd^{2+} and Zn^{2+} in bacterial reaction centers. *Proc. Natl. Acad. Sci. USA* **97**, 1542–1547 (2000).
23. Alexov, E. G. & Gunner, M. R. Calculated protein and proton motions coupled to electron transfer: electron transfer from Q_A^- to Q_B in bacterial photosynthetic reaction centers. *Biochemistry* **38**, 8253–8270 (1999).
24. Rabenstein, B., Ullmann, G. M. & Knapp, E.-W. Electron transfer between the quinones in the photosynthetic reaction center and its coupling to conformational changes. *Biochemistry* **39**, 10487–10496 (2000).
25. Nishikawa, G., Sugo, Y., Saito, K. & Ishikita, H. Absence of electron-transfer-associated changes in the time-dependent X-ray free-electron laser structures of the photosynthetic reaction center. *eLife* **12**, RP88955 (2023).
26. Roszak, A. W. et al. New insights into the structure of the reaction centre from *Blastochloris viridis*: evolution in the laboratory. *Biochem. J.* **442**, 27–37 (2012).
27. Kawashima, K. & Ishikita, H. Energetic insights into two electron transfer pathways in light-driven energy-converting enzymes. *Chem. Sci.* **9**, 4083–4092 (2018).
28. Prince, R. C. & Dutton, P. L. The primary acceptor of bacterial photosynthesis: its operating midpoint potential? *Arch. Biochem. Biophys.* **172**, 329–334 (1976).
29. Maróti, P. & Wraight, C. W. Flash-induced H^+ binding by bacterial photosynthetic reaction centers: influences of the redox states of the acceptor quinones and primary donor. *Biochim. Biophys. Acta* **934**, 329–347 (1988).
30. McPherson, P. H., Nagarajan, V., Parson, W. W., Okamura, M. Y. & Feher, G. pH-dependence of the free energy gap between DQ_A and $D^+Q_A^-$ determined from delayed fluorescence in reaction centers from *Rhodobacter sphaeroides* R-26. *Biochim. Biophys. Acta* **1019**, 91–94 (1990).
31. Hienerwadel, R. et al. Protonation of Glu L212 following Q_B^- formation in the photosynthetic reaction center of *Rhodobacter sphaeroides*: evidence from time-resolved infrared spectroscopy. *Biochemistry* **34**, 2832–2843 (1995).
32. Nabedryk, E. et al. Fourier transform infrared difference spectroscopy of secondary quinone acceptor photoreduction in proton transfer mutants of *Rhodobacter sphaeroides*. *Biochemistry* **34**, 14722–14732 (1995).
33. Miksovska, J. et al. Distant electrostatic interactions modulate the free energy level of Q_A^- in the photosynthetic reaction center. *Biochemistry* **35**, 15411–15417 (1996).
34. Paddock, M. L., Feher, G. & Okamura, M. Y. Proton transfer pathway and mechanism in bacterial reaction centers. *FEBS Lett.* **555**, 45–50 (2003).
35. Xu, Q. et al. X-ray structure determination of three mutants of the bacterial photosynthetic reaction centers from *Rb. sphaeroides*: altered proton transfer pathways. *Structure* **12**, 703–715 (2004).
36. Ishikita, H. & Knapp, E.-W. Energetics of proton transfer pathways in reaction centers from *Rhodobacter sphaeroides*: the Glu-H173 activated mutants. *J. Biol. Chem.* **280**, 12446–12450 (2005).
37. Ishikita, H. & Knapp, E.-W. Induced conformational change upon Cd^{2+} binding at photosynthetic reaction centers. *Proc. Natl. Acad. Sci. USA* **102**, 16215–16220 (2005).
38. Sebban, P., Maroti, P., Schiffer, M. & Hanson, D. K. Electrostatic dominoes: long distance propagation of mutational effects in photosynthetic reaction centers of *Rhodobacter capsulatus*. *Biochemistry* **34**, 8390–8397 (1995).
39. Schutz, C. N. & Warshel, A. What are the dielectric constants of proteins and how to validate electrostatic models? *Proteins* **44**, 400–417 (2001).
40. Sugo, Y., Saito, K. & Ishikita, H. Mechanism of the formation of proton transfer pathways in photosynthetic reaction centers. *Proc. Natl. Acad. Sci. USA* **118**, e2103203118 (2021).
41. Saito, K., Rutherford, A. W. & Ishikita, H. Mechanism of proton-coupled quinone reduction in Photosystem II. *Proc. Natl. Acad. Sci. USA* **110**, 954–959 (2013).
42. Ishikita, H., Morra, G. & Knapp, E.-W. Redox potential of quinones in photosynthetic reaction centers from *Rhodobacter sphaeroides*: dependence on protonation of Glu-L212 and Asp-L213. *Biochemistry* **42**, 3882–3892 (2003).
43. Okamura, M. Y., Paddock, M. L., Graige, M. S. & Feher, G. Proton and electron transfer in bacterial reaction centers. *Biochim. Biophys. Acta* **1458**, 148–163 (2000).
44. Stowell, M. H. B. et al. Light-induced structural changes in photosynthetic reaction center: implications for mechanism of electron-proton transfer. *Science* **276**, 812–816 (1997).
45. Allen, J. P., Feher, G., Yeates, T. O., Komiya, H. & Rees, D. C. Structure of the reaction center from *Rhodobacter sphaeroides* R-26: the protein subunits. *Proc. Natl. Acad. Sci. USA* **85**, 8487–8491 (1988).
46. Ermler, U., Fritzsch, G., Buchanan, S. K. & Michel, H. Structure of the photosynthetic reaction centre from *Rhodobacter sphaeroides* at 2.65 Å resolution. *Structure* **2**, 925–936 (1994).
47. Flores, M. et al. Protein-cofactor interactions in bacterial reaction centers from *Rhodobacter sphaeroides* R-26: II. Geometry of the hydrogen bonds to the primary quinone $Q_A^{\bullet-}$ by ^1H and ^2H ENDOR spectroscopy. *Biophys. J.* **92**, 671–682 (2007).
48. Brudler, R. et al. Asymmetric binding of the 1- and 4-C=O groups of Q_A in *Rhodobacter sphaeroides* R26 reaction centres monitored by Fourier transform infra-red spectroscopy using site-specific isotopically labelled ubiquinone-10. *EMBO J.* **13**, 5523–5530 (1994).
49. Bao, H., Zhang, C., Ren, Y. & Zhao, J. Low-temperature electron transfer suggests two types of Q_A in intact photosystem II. *Biochim. Biophys. Acta* **1797**, 339–346 (2010).
50. Saito, K., Mino, H., Nishio, S. & Ishikita, H. Protonation structure of the closed-cubane conformation of the O_2-evolving complex in photosystem II. *PNAS Nexus* **1**, pgac221 (2022).
51. Hienerwadel, R. & Berthomieu, C. Bicarbonate binding to the non-heme iron of photosystem II investigated by Fourier transform infrared difference spectroscopy and ^{13}C-labeled bicarbonate. *Biochemistry* **34**, 16288–16297 (1995).
52. Chernev, P., Zaharieva, I., Dau, H. & Haumann, M. Carboxylate shifts steer interquinone electron transfer in photosynthesis. *J. Biol. Chem.* **286**, 5368–5374 (2011).
53. MacKerell, A. D. Jr. et al. All-atom empirical potential for molecular modeling and dynamics studies of proteins. *J. Phys. Chem. B* **102**, 3586–3616 (1998).
54. Brooks, B. R. et al. CHARMM: a program for macromolecular energy minimization and dynamics calculations. *J. Comput. Chem.* **4**, 187–217 (1983).
55. Rabenstein, B., Ullmann, G. M. & Knapp, E.-W. Calculation of protonation patterns in proteins with structural relaxation and molecular ensembles - application to the photosynthetic reaction center. *Eur. Biophys. J.* **27**, 626–637 (1998).
56. Bashford, D. & Karplus, M. pK_a's of ionizable groups in proteins: atomic detail from a continuum electrostatic model. *Biochemistry* **29**, 10219–10225 (1990).
57. Nozaki, Y. & Tanford, C. Acid-base titrations in concentrated guanidine hydrochloride. Dissociation constants of the guanidinium ion and of some amino acids. *J. Am. Chem. Soc.* **89**, 736–742 (1967).
58. Tanokura, M. ^1H nuclear magnetic resonance titration curves and microenvironments of aromatic residues in bovine pancreatic ribonuclease A. *J. Biochem.* **94**, 51–62 (1983).

59. Tanokura, M. ^{1}H-NMR study on the tautomerism of the imidazole ring of histidine residues: I. Microscopic p*K* values and molar ratios of tautomers in histidine-containing peptides. *Biochim. Biophys. Acta* **742**, 576–585 (1983).
60. Tanokura, M. ^{1}H-NMR study on the tautomerism of the imidazole ring of histidine residues: II. Microenvironments of histidine-12 and histidine-119 of bovine pancreatic ribonuclease a. *Biochim. Biophys. Acta* **742**, 586–596 (1983).
61. Rabenstein, B. & Knapp, E.-W. Calculated pH-dependent population and protonation of carbon-monoxy-myoglobin conformers. *Biophys. J.* **80**, 1141–1150 (2001).
62. Bashford, D. & Karplus, M. pK_as of ionizable groups in proteins - atomic detail from a continuum electrostatic model. *Biochemistry* **29**, 10219–10225 (1990).
63. Cotton, T. M. & van Duyne, R. P. An electrochemical investigation of the redox properties of bacteriochlorophyll and bacteriopheophytin in aprotic solvents. *J. Am. Chem. Soc.* **101**, 7605–7612 (1979).
64. Kishi, S., Saito, K., Kato, Y. & Ishikita, H. Redox potentials of ubiquinone, menaquinone, phylloquinone, and plastoquinone in aqueous solution. *Photosynth. Res.* **134**, 193–200 (2017).
65. QSite. (2012), version 5.8, Schrödinger, LLC, New York, NY.
66. Jorgensen, W. L., Maxwell, D. S. & Tirado-Rives, J. Development and testing of the OPLS all-atom force field on conformational energetics and properties of organic liquids. *J. Am. Chem. Soc.* **118**, 11225–11236 (1996).

Acknowledgements

This research was supported by JSPS KAKENHI (JP23H04963 and JP24K01986 to K.S.; JP20H03217 and JP23H02444 to H.I.) and the Interdisciplinary Computational Science Program in CCS, University of Tsukuba.

Author contributions

H.I. designed research; T.N. performed computations; T.N., K.S, and H.I. analyzed data; and H.I. wrote the paper.

Competing interests

The authors declare no competing interest.

Additional information

Supplementary information The online version contains supplementary material available at https://doi.org/10.1038/s42004-024-01281-5.

Correspondence and requests for materials should be addressed to Hiroshi Ishikita.

Peer review information *Communications Chemistry* thanks Muhamed Amin, Chunxi Zhang and the other, anonymous, reviewer(s) for their contribution to the peer review of this work.

Reprints and permissions information is available at http://www.nature.com/reprints

Publisher's note Springer Nature remains neutral with regard to jurisdictional claims in published maps and institutional affiliations.

Open Access This article is licensed under a Creative Commons Attribution-NonCommercial-NoDerivatives 4.0 International License, which permits any non-commercial use, sharing, distribution and reproduction in any medium or format, as long as you give appropriate credit to the original author(s) and the source, provide a link to the Creative Commons licence, and indicate if you modified the licensed material. You do not have permission under this licence to share adapted material derived from this article or parts of it. The images or other third party material in this article are included in the article's Creative Commons licence, unless indicated otherwise in a credit line to the material. If material is not included in the article's Creative Commons licence and your intended use is not permitted by statutory regulation or exceeds the permitted use, you will need to obtain permission directly from the copyright holder. To view a copy of this licence, visit http://creativecommons.org/licenses/by-nc-nd/4.0/.

© The Author(s) 2024